DESIGN AND CALIBRATION OF CHAMBERS FOR THE MEASUREMENT OF HOUSED DAIRY COW GASEOUS EMISSIONS

J. L. Drewry, J. M. Powell, C. Y. Choi

ABSTRACT. *The increased global demand for milk and other dairy products over the past decade has heightened concerns about the potential for increased environmental impacts. Accurate measurement of gas emissions from dairy cows is essential to assess the effects of cow diets and other management practices on both the composition and rate of gas emissions. In this article, methodologies are described to instrument, calibrate, and assess the uncertainty of gas emissions by cows housed in chambers that simulate production settings. The supply and exhaust ducts of each chamber were equipped with pitot tubes, temperature and relative humidity probes, and gas samplers to monitor airflow rates, gas composition, and gas emission rates. A Fourier transform infrared spectroscopy (FTIR) instrument was used to quantify gaseous concentrations in the gas samples on a semi-continuous basis. The measurement uncertainty of the rate of gaseous emission from the chambers was quantified, and gas concentration and differential pressure, as measured by the pitot tubes, were identified as the primary parameters contributing to gas emission uncertainties. Mass recovery tests determined that the recovery of methane from each chamber was within 10% of the released mass. Fan operating curves were experimentally determined to identify optimum differential chamber pressures to minimize gas leakage from the chambers. A computational fluid dynamics model was developed to assess air mixing patterns and define steady-state conditions. The model was validated with experimental data of air velocity within each chamber. These procedures will facilitate accurate measurement of gas emissions from housed dairy cows and provide a laboratory to test various gas mitigation treatments.*

Keywords. *Computational fluid dynamics, Dairy, Emission chamber.*

Demand for milk and other dairy products has been increasing worldwide as human populations increase and standards of living rise. As a result, the environmental impact of large-scale livestock farming has the potential to increase as farms grow larger and increase their output. Production of ammonia and methane from dairy cows is a concern due to the potential of these emissions to reduce environmental quality. Ammonia is volatilized from manure as a function of its nitrogen content, environmental conditions, and handling practices and can lead to the formation of particulate matter, which can be hazardous to human health (Pope et al., 2009). In addition, ammonia can be converted to nitrous oxide, a greenhouse gas, as part of the nitrogen cycle. Methane, a greenhouse gas, is produced through enteric fermentation and manure digestion by specific microorganisms. Scientists and engineers face the challenge of finding methods to mitigate the production of these gasses while, at the same time, increasing dairy production.

Modifying herd management practices and dairy housing design is a common approach for reducing gaseous emissions from cows. It has been established that diet modifications, such as decreasing crude protein content of cow diets from 18% to 16.5%, reduces ammonia emissions without impacting milk production and protein content (Aguerre et al., 2010). In addition, environmental factors, such as temperature and relative humidity, have been shown to affect ammonia emissions from dairy operations (Powell et al., 2008a, 2008b). Furthermore, feed management, rumen modifiers, and breeding can decrease methane emissions (Knapp et al., 2014). However, under production settings, it can be difficult to measure the impact that feed and other factors may have on methane and ammonia emissions because these compounds are volatile.

Researchers are also working to identify strategies to mitigate the effect of gaseous emissions through capture and treatment of the air from animal housing. These technologies will most likely become more economically feasible as farms increase in size. Acid scrubbers have been deployed in many types of animal housing to reduce odor issues from ammonia and other compounds (Melse and Timmerman, 2009). Biological filters are capable of removing and de-

Submitted for review in August 2016 as manuscript number PAFS 12046; approved for publication by the Plant, Animal, & Facility Systems Community of ASABE in May 2017.

Mention of company or trade names is for description only and does not imply endorsement by the USDA. The USDA is an equal opportunity provider and employer.

The authors are **Jessica L. Drewry, ASABE Member,** Graduate Student, Department of Biological Systems Engineering, University of Wisconsin, Madison, Wisconsin; **J. Mark Powell,** Research Scientist, USDA-ARS U.S. Dairy Forage Research Center, Madison, Wisconsin; **Christopher Y. Choi, ASABE Member,** Professor, Department of Biological Systems Engineering, University of Wisconsin, Madison, Wisconsin. **Corresponding author:** Jessica L. Drewry, 460 Henry Mall, University of Wisconsin, Madison, WI 53706; phone: 608-262-3310; e-mail: jdrewry@wisc.edu.

grading many compounds, including methane, from the air through the use of microorganisms and organic material (Ndegwa et al., 2008; Yoon et al., 2009). In addition, researchers have developed, *in silico*, a new material theorized to be capable of removing methane from dilute concentration sources such as barn air (Kim et al., 2013). The ability to test and improve these technologies at a small scale and in controlled setting would be invaluable.

Sealed environmental chambers equipped to derive the flux of mass and thermal energy across the chamber boundaries allow researchers to study methods to mitigate the generation of gaseous emissions from housed dairy cows. Researchers have also used indirect calorimeter hoods to measure enteric methane generation (Nienaber and Maddy, 1985; Place et al., 2011; Freetly and Brown-Brandl, 2013; Maia et al., 2015). Large environmental chambers have also been designed and calibrated to measure the flux of nitrogen at the scale of a full barn (Lefcourt, 2001; Lefcourt et al., 2001; Grainger et al., 2007; Gilhespy et al., 2006). Powell et al. (2007) designed and calibrated four temporary chambers equipped and calibrated to measure nitrogen flux through the environment.

In this study, we document the design of permanent chambers capable of simulating production settings while collecting data on gas emissions over a period of several days. Key design features include four replicate chambers, isolation of the cow from the external environment, and an instrumentation system capable of measuring the mass flux of gasses through the chambers. We propose calibration procedures for the chambers, including estimation of measurement uncertainty. Finally, we developed a computational fluid dynamics model capable of assessing mixing patterns within the chambers to guide experimental sensor placement and appropriate data collection periods. These chambers could be used to identify practices to reduce gaseous emissions from dairy cows as well as to test mitigation strategies.

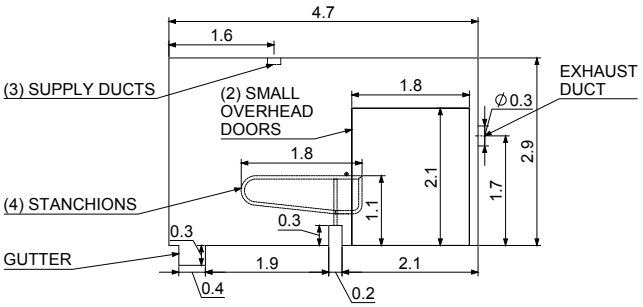

Figure 1. Side view of single chamber (all dimensions in meters).

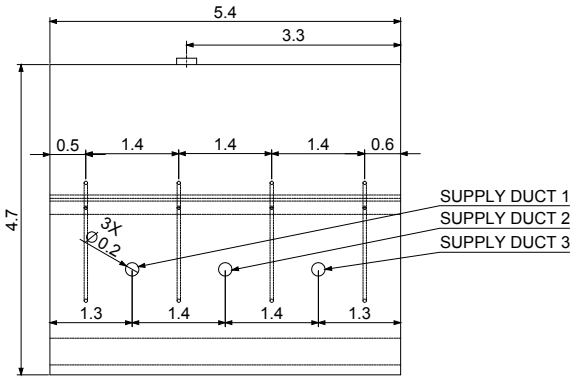

Figure 2. Top view of single chambers (all dimensions in meters).

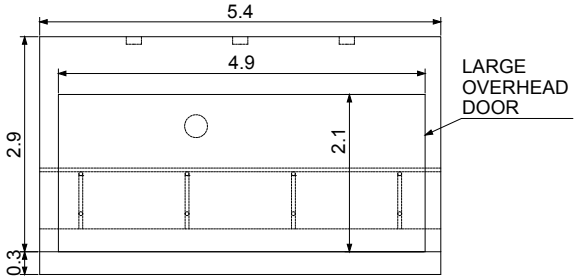

Figure 3. Front view of single chambers (all dimensions in meters).

MATERIALS AND METHODS

CHAMBER DESIGN

To provide a suitable permanent field laboratory, four 3-cow emission chambers and a control room were remodeled in an existing facility at the USDA-ARS Dairy Forage Research Center in Prairie du Sac, Wisconsin (Powell et al., 2007). The chambers were designed to accommodate research while retaining as many production setting features as possible. The chambers are located at one end of a barn and can be isolated, via an overhead door, from the other end of the barn. Cows are housed in the chamber, except when taken to the milking parlor, three times per day.

Each chamber measures approximately 4.7 m deep × 5.4 m wide × 2.9 m high; all dimensions are shown in figures 1, 2, and 3. The chamber walls were constructed of concrete masonry units and coated with 65 mil polyurea spray coating (Volatile Free, Inc., Brookfield, Wisc.) to reduce sorption of ammonia to the walls and allow ease of cleaning between experiments. Industrial-grade, insulated overhead doors were installed to allow ease of access to the cows for feeding and milking while minimizing air infiltration into the chambers when closed. Large overhead doors (one per chamber) were located behind the gutter to allow access to the cows, while small overhead doors (two per chamber) were located on both sides of the feed alley to allow access for feeding. The tie-stalls were bedded with rubber mats (Unicup Softbed, Kraiburg, Germany) and sloped to facilitate drainage into the common manure gutter. The gutter was sealed from the exterior using a block of plastic-wrapped foam that conforms to the gutter shape.

CHAMBER VENTILATION

A single, forward curve, 0.62 m diameter, 1.5 hp blower (model 3C010, Dayton, Chicago, Ill.) provided ventilation of conditioned air to the four chambers though ductwork in the attic above the chambers (figs. 4 and 5). The blower was controlled by a variable-frequency drive (model GS2 AC, Automation Direct, Atlanta, Ga.). Additionally, an inline 72 kW electric heater (model DFP 300, Modine, Racine, Wisc.) was located within the supply duct to condition the air. The ductwork was designed to accommodate existing building design features. Twelve 0.2 m diameter supply

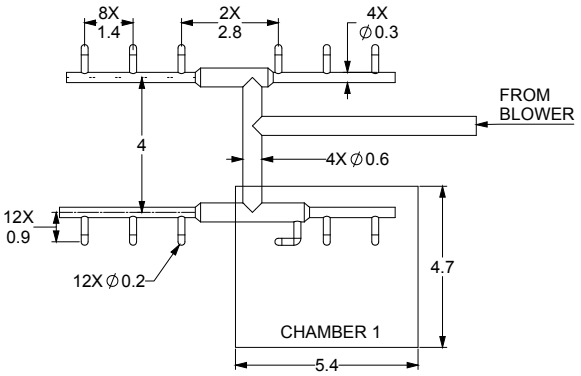

Figure 4. Top view of ventilation system including the outline of chamber 1 (all dimensions in meters).

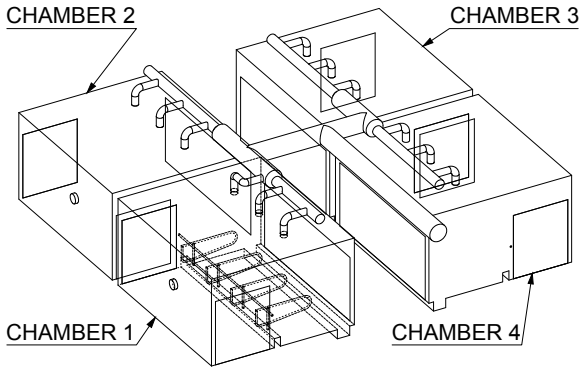

Figure 5. Isometric view of chambers and ventilation assembly. Interior lines of chambers 2 through 4 are hidden for clarity.

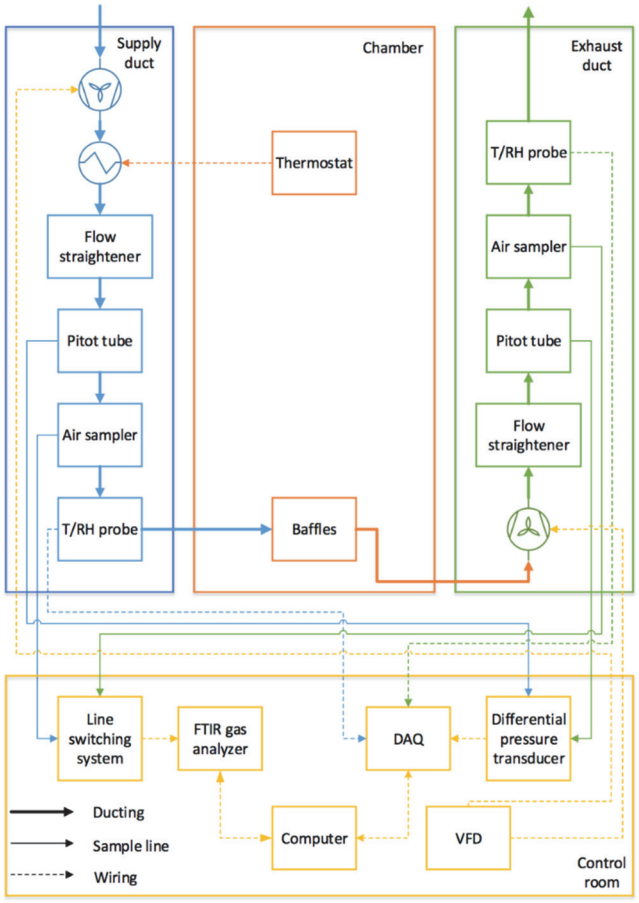

Figure 6. System instrumentation schematic for a single chamber. All chambers share a single supply duct and have individual exhaust ducts.

ducts (three per chamber) were manually balanced to within 10% of each other by adjusting dampers at each chamber supply duct. The dampers were located just after the branch from the main duct, before the 90° turn into the chamber.

Inline 0.5 hp exhaust fans (model TD-315, Soler and Palau, Jacksonville, Fla.) were used to expel air from the chambers into 0.31 m diameter ductwork housing the sensors. External ductwork was insulated to prevent condensation and freezing of water vapor inside the sample lines. The exhaust fans were set manually, using a variable-frequency drive (model 215F, Northwest Envirofan, Oshkosh, Wisc.) to maintain a higher mass flow rate than the supply to prevent gas leakage to the exterior. Variable-frequency drives were used for both the supply and exhaust fans to allow the chambers to be operated under a wider range of environmental conditions while ensuring cow comfort.

Chamber Instrumentation

The chambers were outfitted with several sensors to calculate mass flow rate and measure gas concentrations entering and exiting the chambers (fig. 6). The exhaust duct of each chamber contained a stainless steel, equal area, transverse pitot tube (Ultraprobe AMPS, Ultratech Industries, Inc., Garner, N.C.). The pitot tubes were placed behind a flow straightener and a minimum of ten diameters of uninterrupted duct flow from the exhaust fan to ensure fully developed flow before measurement. The outlet ducts also contained a custom-fabricated, 24-point, equal-area, cross-sectional air sampler. In addition, a temperature and relative humidity probe was located in the outlet duct of each chamber (HC2S3, Campbell Scientific, Logan, Utah). Measurements from the pitot tubes and temperature and relative humidity probes were taken every 500 ms and stored as 1 min averages (model CR5000, Campbell Scientific, Logan, Utah). The supply duct was identically outfitted with a pitot tube, air sampler, and temperature and relative humidity probe.

The pitot tube and air sample lines originating from both the supply and exhaust ducts were run to a temperature-controlled room where the sensor equipment, data acquisition device, and computer were located. The pitot tube lines were run to pressure transducers (model 264, Setra, Boxborough, Mass.) that measured the difference between total and static pressure obtained from the pitot tubes to yield air velocity. The pitot tube lines were flushed regularly with compressed air to prevent the accumulation of dust. Teflon tubing (3.2 mm i.d.) was used for all air sample lines to prevent sample contamination from outgassing (Nalgene, Rochester, N.Y.). The air sample lines were run to a custom six-line switching system (Gasmet) that was connected to a Fourier transform infrared (FTIR) gas analyzer (model DX4015, Gasmet, Finland). Sample line filters (model 6723-5000, Whatman, Pittsburgh, Pa.) were installed to prevent dust and moisture from entering the FTIR sensor. Under standard operating conditions, the FTIR sample cell was flushed for 40 s prior to the sample, followed by three consecutive 20 s measurements. All gas samples were analyzed using Calcmet software (Calcmet, 2013).

CHAMBER OPERATION

A mass balance was performed on each chamber to determine the rate of gaseous generation (m_{gen}, kg):

$$m_{in} - m_{out} + m_{gen} = m_{acc} \quad (1)$$

where

m_{in} = mass of gas entering the chamber (kg)
m_{out} = mass of gas exiting the chamber (kg)
m_{acc} = mass of accumulated gas (kg).

Under steady-state conditions, the accumulation of gas can be assumed to be zero. The mass flux into the chamber was the sum of the supply ventilation and infiltration rates. The mass flux of gas into (from the supply duct) or out of the chamber ($\dot{m}_{in}, \dot{m}_{out}$, kg s^{-1}) was calculated as:

$$\dot{m}_{in}, \dot{m}_{out} = \left(\frac{2\Delta p}{\rho}\right)^{\frac{1}{2}} \frac{AxM}{V_m} 10^{-6} \quad (2)$$

where

Δp = pressure difference from the pitot tube (Pa)
ρ = air density (kg m^{-3})
A = duct area (m^2)
x = gas concentration in parts per million by volume (ppmv)
V_m = molar volume corrected for environmental conditions (m^3 mol^{-1})
M = molecular mass of the gas (kg mol^{-1}).

The infiltration rate mass flux ($\dot{m}_{inf}$) was calculated as:

$$\dot{m}_{inf} = \frac{IVxM}{V_m} 10^{-6} \quad (3)$$

where I is the infiltration rate (s^{-1}), and V is the chamber volume (m^3). The moist air density and molar volume were adjusted to account for environmental conditions of temperature, atmospheric pressure, and relative humidity (ASHRAE, 2009). The total mass of gas entering and exiting the chamber was calculated by numerically integrating the mass flux over the experimental time period using the trapezoidal rule and can then be used to solve for the mass of generated gas in equation 1.

CHAMBER CALIBRATION

Prior to calibration, the seals of the chamber overhead doors (three per chamber) and windows were visually inspected using mineral oil smoke from an insect fogger. All visible leaks under standard operating conditions were sealed prior to the start of calibration. For all calibration experiments, steady-state conditions were assumed after six air exchanges, doubling the time for a perfectly mixed system.

Leakage Calibration

Potential gas leakage into the chambers from the surroundings was quantified using a negative step test. The concentration of a gas as a function of time, after a stepwise forcing function, can be modeled as follows (Charlesworth, 1988):

$$C(t) = C_\infty + \frac{F}{Q} + \left(C_0 - C_\infty - \frac{F}{Q}\right) e^{-tI} \quad (4)$$

where

$C(t)$ = mass fraction of tracer
C_∞ = background mass fraction of tracer
C_0 = initial mass fraction of tracer
F = generation rate of tracer material in control volume (m^3 s^{-1})
Q = volumetric flow rate through control volume (m^3 s^{-1})
t = time (s)
I = infiltration rate (s^{-1}).

The dimensionless concentration (C^*) can be described as follows:

$$C^* = \frac{C(t) - C_\infty}{C_0 - C_\infty} \quad (5)$$

The experimental procedure was adapted from Purswell et al. (2006). The negative step test was performed on each chamber at three operating pressures to develop a relationship between infiltration rate and chamber differential pressure between the chambers and the barn in which they are housed. The order of the tests was randomized prior to the start of the experiment.

Throughout the experiment, gas concentration was measured in the exhaust duct of the experimental chamber and in the alley between the chambers. First, the pressure difference between the chambers and the barn under standard operating conditions was recorded to serve as a baseline. All supply ducts to the chamber were sealed, and the exhaust fans were adjusted to achieve the desired differential operating pressure for the specific test. Carbon dioxide was then diffused into the chamber using perforated PVC piping (0.013 m diameter) installed at the ceiling of the chamber. Gas injection into the chamber was controlled using a single-stage pressure regulator (0 to 400 kPa, Fisher Scientific, Waltham, Mass.). Once a steady-state concentration of carbon dioxide was achieved (as monitored by the FTIR), the cylinder was closed and the outlet concentration of carbon dioxide was monitored until levels returned to background concentrations. Gas concentration, temperature, relative humidity, and mass flow rate were monitored and recorded for the duration of the experiment, as described earlier. The infiltration rate was calculated using a nonlinear regression of carbon dioxide concentration as a function of time (eq. 4) in the MATLAB Curve Fitting Toolbox using the robust trust-region algorithm (MATLAB, 2015). The algorithm accounted for outliers, which arose due to the imperfect mixing within the chambers.

Mass Recovery Calibration

The mass recovery of controlled amounts of gas released into the chambers was quantified experimentally. Ultra-high purity methane was released into the chamber from a gas cylinder controlled by both a single-stage pressure regulator (model 996SS, Harris, Mason, Ohio) and a flowmeter (0-10 SCFH, Cole-Parmer, Vernon Hills, Ill.). Perforated tubing (3.2 mm i.d.) was used to diffuse the gas inside the chamber from the stanchions to simulate methane production from

cows. The FTIR gas analyzer was set to sample in both the supply and exhaust ducts of the chamber for the duration of the experimental period, until the chamber returned to background concentrations or at least six air exchanges had elapsed. In addition, temperature, relative humidity, and volumetric flow rate were recorded in the supply and exhaust ducts of the chamber for the duration of the experiment. The mass of the gas cylinder was measured prior to and immediately after gas release into the chamber on a scale with accuracy to 0.1 g. This procedure was repeated three times for each chamber. The known mass of methane released was then compared with the calculated mass released using equation 1.

Airflow Measurements

One of the four chambers (chamber 2) was selected for detailed airflow measurements at the chamber supply duct, exhaust duct, and interior. Replicate measurements were collected over three consecutive days. The velocity at the supply duct and exhaust duct was characterized using a hot-wire anemometer (Velometer AVM440, Alnor, Shoreview, Minn.), with measurement locations selected using the log-Tchebycheff method to sample within equal-area circles to derive a volumetric flow rate (fig. 7) (ASHRAE, 2009). One-second measurements were recorded over a period of 1 min. Interior velocity magnitude and direction were measured using an ultrasonic anemometer (model 8100, R.M. Young Co., Traverse City, Mich.). One-second measurements were recorded for three consecutive 5 min intervals at 15 locations within the chamber, to ensure one replicate of data could be collected per day, from which the average and standard deviation were calculated. Measurements were taken at heights of 1.4, 1.7, and 2.1 m at five locations: at the centerlines of supply ducts 1 through 3, 1.3 m from the sidewall and in the center of the feed alley, and 2.1 m from the sidewall and in the center of the feed alley. Measurements were recorded after steady-state conditions were reached in the chamber, as determined by convergence of the 1 min and 5 min averages of velocity.

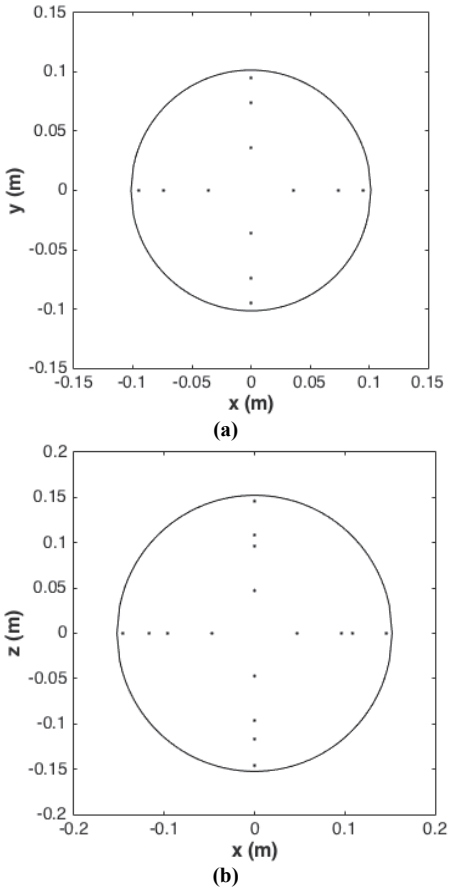

Figure 7. Measurement locations for (a) supply duct as seen from above the chamber (plan view) and (b) exhaust duct as seen from inside the chamber (side view).

MEASUREMENT UNCERTAINTY ANALYSIS

The contribution of each measured parameter to the standard uncertainty of the mass flux into and out of the chamber was estimated. The gas constant and molecular mass were assumed to have a negligible contribution to standard uncertainty. The root sum square (RSS) error of the combined uncertainties in the mass flux ($\Delta\dot{m}$) can be described as follows (Taylor and Kuyatt, 1994):

$$\Delta\dot{m} = \sqrt{\left(\frac{\partial\dot{m}}{\partial x_m}\Delta x_m\right)^2 + \left(\frac{\partial\dot{m}}{\partial T}\Delta T\right)^2 + \left(\frac{\partial\dot{m}}{\partial\delta P}\Delta\delta P\right)^2 + \left(\frac{\partial\dot{m}}{\partial RH}\Delta RH\right)^2} \quad (6)$$

where

Δx_m = absolute standard uncertainty in gas concentration (ppmv)

ΔT = absolute standard uncertainty in dry-bulb temperature (K)

$\Delta\delta P$ = absolute standard uncertainty in differential pressure (Pa)

ΔRH = absolute standard uncertainty in relative humidity.

The absolute standard uncertainties for temperature, relative humidity, and differential pressure were determined based on manufacturer calibrations of the sensors. The absolute standard uncertainty of the gas concentration was calculated by a third-party entity that certified the equipment (TÜV Rheinland, 2013). The partial derivatives of equation 4 were evaluated using MATLAB (2015). The RSS error of the mass flux (Δm, kg) was numerically integrated over the duration of the experiment to yield the uncertainty of the mass of gas generated:

$$\Delta m = \sqrt{\left(\frac{1}{2}\sum_{i=1}^{N-1}\left(t_{i+1}-t_i\right)\left(\Delta\dot{m}_i + \Delta\dot{m}_{i+1}\right)\right)^2} \quad (7)$$

where N is the number of measurements, and t is the time at measurement. The uncertainty in the measurement of mass entering, exiting, and accumulating in the chamber was summed to give the final uncertainty in the generation of mass within the chamber. The contribution of each parameter to the standard uncertainty was estimated as follows (Taylor and Kuyatt, 1994):

$$C_a = \frac{\left(\frac{\partial\dot{m}}{\partial a}\Delta a\right)^2}{\left(\Delta\dot{m}\right)^2} \quad (8)$$

where a is the standard uncertainty of the parameter of interest, and C_a is the contribution of an individual parameter to the standard uncertainty (%).

Computational Fluid Dynamics Model

Computational fluid dynamics (CFD) was used to model the transport of mass and momentum within the domain (ANSYS, 2011). The governing equations of the simulation are as follows:

$$\nabla \cdot \mathbf{v} = 0 \tag{9}$$

$$\mathbf{v} \cdot \nabla \mathbf{v} = -\frac{1}{\rho}\nabla p + \nu \nabla^2 \mathbf{v} \tag{10}$$

where

$\mathbf{v}$ = velocity vector (m s^{-1})

ρ = fluid density (kg m^{-3})

p = pressure (Pa)

ν = fluid kinematic viscosity (m^2 s^{-1}).

The geometry was created to replicate the single chamber in which the velocity measurements were collected, as described earlier for the chamber calibration methods. However, the presence of the stanchions was neglected in simulations. To achieve the desired resolution, the geometry was divided into sections to allow a finer mesh in the area under the jet and next to the wall to fully resolve the large gradients that can occur in those regions. A predominately tetrahedral mesh of approximately two million cells was created to ensure proper resolution of the boundary conditions and jet development. The mesh was refined at the walls to ensure that values of y+, the dimensionless distance from the wall, were less than 100. The experimental data collected at the supply duct inlet, using a hot-wire anemometer, were used to define the supply duct boundary conditions. Simulations were performed applying the experimental velocity data, through user-defined functions, or a mass flow rate derived from the velocity and environmental data. Turbulence parameters at the inlet were defined assuming fully developed duct flow (ANSYS, 2011). The outlet was simulated as an outflow condition. The Reynolds stress turbulence model, with enhanced wall functions, was used to better capture the turbulence within the enclosed domain (Norton, 2007). Second-order spatial discretization and the Simple pressure interpolation scheme were employed. Convergence was monitored based on the change in mean and maximum velocity in the domain as well as along the centerline of the center jet (supply duct 2).

Results and Discussion

Chamber Calibration

Infiltration rate was determined for each chamber as a function of differential pressure from the leakage calibration data. Due to the lack of automated control of the exhaust fans, it was difficult to maintain a constant chamber pressure, and average values of pressure difference during the experiment were recorded. The experimental data were summarized as plots of the dimensionless concentration of carbon dioxide as a function of time for each chamber (fig. 8). The differences in experimental times are related to the combination of the absolute concentration of carbon dioxide released into the chamber and the exhaust fan flow rate; higher gas concentrations and lower flow rates resulted in longer experimental times. A trust-region algorithm was used to evaluate the fit of the model, along with 95% confidence intervals, of mass fraction as a function of time for each test (table 1). The infiltration rate for each chamber as a function of differential pressure was used to develop operating curves for each chamber (fig. 9). The pressure in chamber 3 was the most difficult to control over the duration of the experiment due to the effect of wind, and thus the results of infiltration rate as a function of differential pressure could be biased due to those fluctuations in pressure (fig. 9c). The curves allow calculations of leakage rate during future experiments to more accurately calculate mass balances in the chambers and reduce measurement uncertainty.

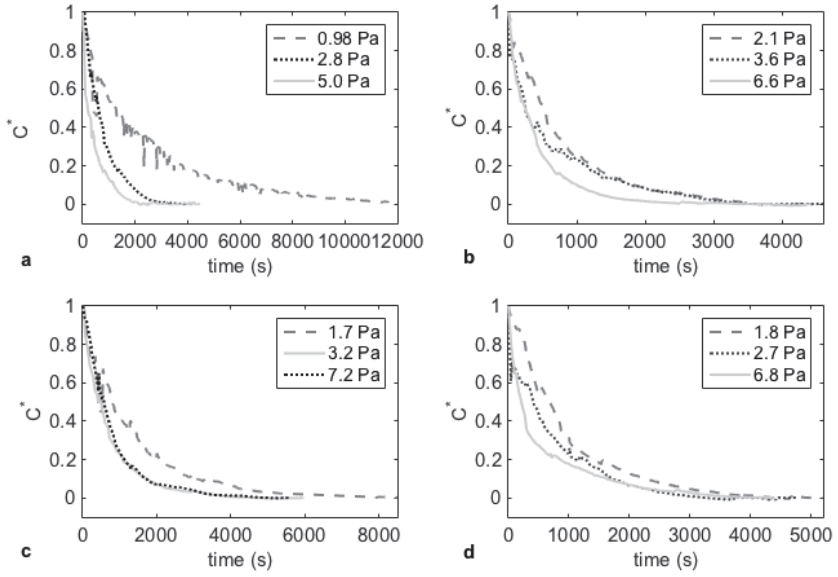

Figure 8. Non-dimensional concentration as a function of time and differential pressure for chambers (a) 1, (b) 2, (c) 3, and (d) 4.

Table 1. Infiltration rate (I, s^{-1}), along with parameter fits for each chamber.

Chamber	Differential Pressure (Pa)	Infiltration Rate (I) (s^{-1})	95% Confidence Interval	Adjusted R^2	RMSE (ppmv)
1	0.978	0.000356	(0.0003559, 0.0003576)	0.999	38.8
	2.76	0.00132	(0.001317, 0.001322)	0.999	14.2
	5.02	0.00190	(0.001807, 0.0019)	0.993	66.6
2	2.08	0.00125	(0.001242, 0.001254)	0.999	16.1
	3.60	0.00139	(0.001321, 0.001449)	0.973	113
	6.57	0.00223	(0.002231, 0.002224)	0.999	14.2
3	1.71	0.000722	(0.0007168, 0.0007263)	0.999	44.3
	3.22	0.00131	(0.001306, 0.001314)	0.999	13.6
	7.18	0.00142	(0.001414, 0.01422)	0.999	13.9
4	1.79	0.001026	(0.001022, 0.00103)	0.999	16.1
	2.72	0.00117	(0.001165, 0.001181)	0.999	16.2
	6.80	0.00198	(0.001855, 0.002101)	0.954	159

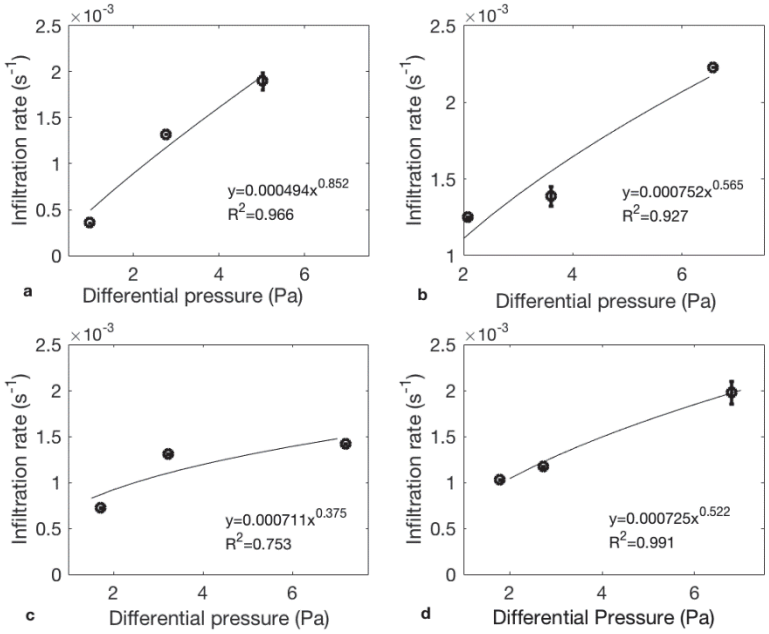

Figure 9. Infiltration rate, along with 95% confidence intervals, as a function of chamber differential pressure, along with power law fit for chambers (a) 1, (b) 2, (c) 3, and (d) 4.

The results of the gas recovery experiments are summarized in table 2, along with the associated measurement uncertainty. The mass of recovered methane was found to be within the measurement uncertainty of the released methane. The percent recovery ranged from 98% to 111%, which is similar to other published values (Lefcourt 2001; Powell et al., 2007; Place et al., 2011; Maia et al., 2015).

Table 2. Experimental results of methane recovery for all chambers.

Chamber	Methane Released (±0.06 g)	Methane Recovered (g)	Measurement Uncertainty (g)	Percent Recovery (%)
1	14.5	14.6	1.2	101
	12.6	13.1	1.8	104
	5.8	5.77	1.1	99
2	16.9	17.2	1.4	102
	11.0	11.9	1.4	108
	5.9	6.55	1.3	111
3	11.8	11.6	1.2	98
	10.5	11.4	1.3	109
	5.1	5.01	1.1	98
4	11.9	12.1	1.3	102
	11.0	12.2	1.1	111
	5.5	5.68	1.1	103

Measurement uncertainty was calculated for four scenarios covering a range of expected values for gas concentrations and ventilation rates (table 3). These scenarios assumed a zero background concentration of methane and neutral pressure (zero differential pressure) operation. The chamber ventilation, as measured by the pressure difference derived from the pitot tube, and gas concentration were found to have the largest contributions to uncertainty. The smallest percent uncertainty (1.5%) in the generation rate of methane occurred at high ventilation rate and high methane concentration. The percent uncertainty for the chambers was similar to the values of 3.9% to 15.8% reported by Maia et al. (2015). Researchers can use the estimation of measurement uncertainty to ensure statistically significant differences between experimental treatments.

The average velocities, along with the standard deviations, at the supply ducts are listed in table 4. Velocity data measured at the supply and exhaust ducts were consistent with the geometry of the ductwork; for each supply duct, the magnitude was found to be higher along the outside edges of turns (sample locations 1-3 and 10-12) and decreased as the

Table 3. Estimated standard uncertainty contribution for each parameter in the measurement of methane generation rate, for four scenarios (two levels of gas concentration and ventilation rate, as measured by the pitot tube differential pressure).

			Uncertainty		
			Δ	%Δ	Percent
Parameter	Unit	Value	(Standard)	(Percent)	Contribution[a]
$\dot{m}$	g s^{-1}	1.30E-04	5.80E-06	4.5	-
x_m	ppmv	20	0.7[b]	3.5	56
T	K	298	0.1[c]	0.034	6.70E-04
RH	%	50	0.8[c]	1.6	7.20E-04
Δp	Pa	9.96	0.6225[d]	6.3	44
$\dot{m}$	g s^{-1}	7.50E-04	2.40E-05	3.2	-
x_m	ppmv	120	0.7	0.58	3.4
T	K	298	0.1	0.034	1.50E-03
RH	%	50	0.8	1.6	1.60E-03
Δp	Pa	9.96	0.6225	6.3	97
$\dot{m}$	g s^{-1}	1.10E-03	1.70E-05	1.5	-
x_m	ppmv	120	0.7	0.58	15
T	K	298	0.1	0.034	6.50E-03
RH	%	50	0.8	1.6	7.00E-03
Δp	Pa	22.4	0.6225	2.8	85
$\dot{m}$	g s^{-1}	1.90E-04	7.10E-06	3.7	-
x_m	ppmv	20	0.7	3.5	86
T	K	298	0.1	0.034	1.00E-03
RH	%	50	0.8	1.6	1.10E-03
Δp	Pa	22.4	0.6225	2.8	14

[a] Due to rounding, values may not sum to total.
[b] Uncertainty from FTIR gas analyzer (DX4015, Gasmet).
[c] Uncertainty from temperature-humidity sensor (HC2S3, Campbell Scientific).
[d] Uncertainty from differential pressure measurement (Ultraprobe AMPS, Ultratech Industries; and model 264, Setra).

duct extended away from the supply fan. The velocity magnitude at the outlet was found to be more uniform due to fewer bends and the lack of branching in the ductwork. The velocity data and calculated mass flow rates through the supply ducts were used as inputs for the CFD modeling. Along with the chamber calibration and uncertainty analysis, careful statistical design of experiments using the chambers can be used to control sources of nuisance variability (Aguerre et al., 2011).

COMPUTATIONAL FLUID DYNAMICS MODEL

The velocity profiles generated by the three-dimensional CFD model were benchmarked against data collected using an ultrasonic anemometer in chamber 2. The simulated velocity along the centerline of each jet was plotted along with the experimental data of the velocity magnitude along the centerline of the jet at three heights: 1.4, 1.7, and 2.1 m (fig. 10). The simulated values agreed with the experimental data, falling within one standard deviation of the experimental data. The large standard deviations in the experimental data were expected due to the heavily branched nature of the ductwork combined with the effect of wind on the supply fan. The measured velocity distribution for supply duct 3 was the least uniform and had the highest standard deviations, which led to the more pronounced differences between the velocity and mass flow inlet boundary conditions. Defining the supply ducts as mass flow inlets, rather than applying the measured velocity profiles, substantially reduced the computational time without substantially affecting the overall simulation results. The mass flow and velocity inlet boundary conditions both resulted in the same overall mass flow rate but differed in the distribution of velocity within the supply duct.

Table 4. Experimental results of average velocity magnitudes and standard deviations at chamber inlets for chamber 2. Measurement locations (*x* and *y*) correspond to a log-T sampling distribution (fig. 7).

Supply Duct	Average Velocity (m s^{-1})	Standard Deviation (m s^{-1})	Sample Location	*x* (m)	*y* (m)
1	3.7	0.24	1	0.095	0
	3.8	0.37	2	0.074	0
	3.3	0.21	3	0.036	0
	3.1	0.46	4	-0.036	0
	2.7	0.46	5	-0.074	0
	2.2	0.75	6	-0.095	0
	3.4	0.46	7	0	-0.095
	3.3	0.7	8	0	-0.074
	3.2	0.53	9	0	-0.036
	3.4	0.38	10	0	0.036
	3.4	0.41	11	0	0.074
	2.6	0.44	12	0	0.095
2	3.4	0.68	1	0.095	0
	3	0.7	2	0.074	0
	2.8	0.82	3	0.036	0
	3.2	0.92	4	-0.036	0
	2	1.4	5	-0.074	0
	1.8	1.5	6	-0.095	0
	2.7	0.98	7	0	-0.095
	3.1	0.98	8	0	-0.074
	2.6	1.2	9	0	-0.036
	2.9	1.3	10	0	0.036
	3.1	1.5	11	0	0.074
	3.1	1.7	12	0	0.095
3	2.8	0.66	1	0.095	0
	2.6	0.73	2	0.074	0
	2.6	0.84	3	0.036	0
	2.6	1	4	-0.036	0
	1.9	1.3	5	-0.074	0
	1.7	1.6	6	-0.095	0
	2.2	0.98	7	0	-0.095
	2.6	1.1	8	0	-0.074
	2.6	1.2	9	0	-0.036
	2.7	1.3	10	0	0.036
	2.8	1.5	11	0	0.074
	2.9	1.7	12	0	0.095

The CFD model was then used to generate velocity vectors and profiles within the chamber to gain insight into mixing patterns within the chamber on planes intersecting a supply duct and an exhaust duct (fig. 11). The potential for dead zones to form within the chamber supports the use of six air exchange rates as a criterion for steady-state conditions, as used in the chamber calibration procedures.

CONCLUSIONS

The emission chambers designed in this study provide a means to study the effects of diet and management practices on greenhouse gas production from housed dairy cows in a controlled setting. Experiments to determine gas recovery and leakage rates confirmed the expected operation of the chambers. However, the pressure difference between the chambers and the alley should be monitored to minimize leakage rates and reduce experimental error. Nevertheless, the measurement uncertainty of gas generation in the chambers was found to be within 1.5% to 4.5% of the gas generation rate and was strongly dependent on the uncertainty in

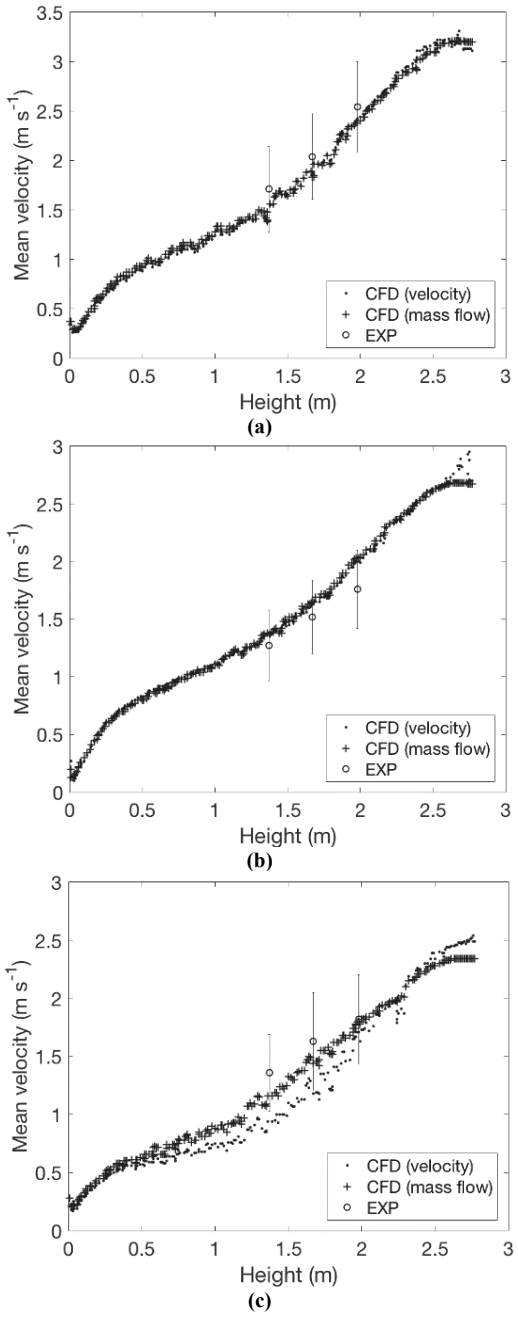

Figure 10. Jet velocity, along the jet centerline, as a function of height for computational fluid dynamics results considering both a velocity inlet boundary conditions (CFD velocity) and a mass flow boundary condition (CFD mass flow) and experimental data (EXP) for supply ducts (a) 1, (b), 2, and (c) 3. CFD simulations were conducted for cases considering the supply duct inlets as velocity and mass flow inlets. The error bars correspond to one standard deviation of the experimental data.

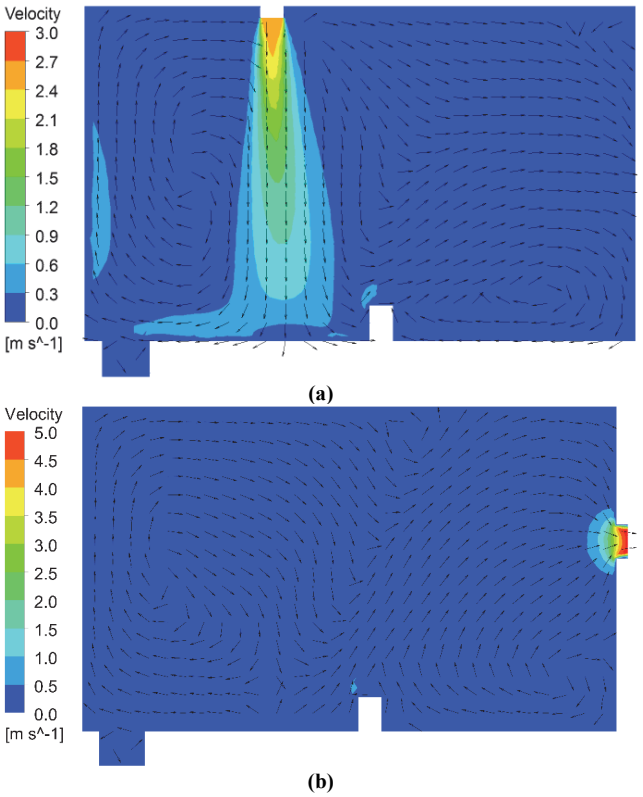

Figure 11. Contours of velocity overlaid with normalized tangential velocity vectors along (a) the centerline of supply duct 2 and (b) the plane along the centerline of the exhaust duct, from the three-dimensional simulation.

measurements of gas concentration and mass flow rate. In addition, the measurement uncertainty, as a percentage of the emission rate, was found to decrease with increasing generation rates, especially if the mass flow rate increased as well.

The computational fluid dynamics simulations were capable of replicating the experimentally measured velocity within the chamber, without a cow present. Optimal boundary conditions were identified to reduce the computational load while generating accurate data. The data generated by the CFD model elucidated the mixing patterns within the barn to better understand mixing patterns and optimal sensor placement. In addition, optimized mixing can reduce the time to steady-state conditions in the chamber, thereby increasing the amount of data that can be collected from the chambers. Future work should focus on expanding the CFD model to include gas species generation and transport within the chamber such that the model can be used to develop and evaluate mitigation strategies.

Installing additional sensor instrumentation and control would improve the performance of the chambers. Specifically, sensors to measure mass flow rate into each chamber separately would improve measurement accuracy. In addition, a plenum could be placed at the supply and exhaust ducts to minimize pressure fluctuations due to external weather conditions. Finally, mixing fans could be installed in the chambers to ensure optimal gas recovery.

After the calibration and uncertainty analysis detailed herein, the chambers can be operated in a manner to minimize experimental error and maximize data collection. These chambers are beneficial in that they can be operated over a period of several days, with only brief breaks in data collection for milking and feeding. We recommend that chambers such as these be used to evaluate the effects of diet on gas generation and to evaluate mitigation strategies in simulated production settings.

ACKNOWLEDGEMENTS

The authors would like to acknowledge the assistance of

Alicia Pelletier in chamber development, maintenance, and experimental data collection. This material is based in part on work supported by the USDA National Institute of Food and Agriculture under Grant No. WIS01898.

REFERENCES

Aguerre, M. J., Wattiaux, M. A., Hunt, T., & Larget, B. R. (2010). Effect of dietary crude protein on ammonia-N emission measured by herd nitrogen mass balance in a freestall dairy barn managed under farm-like conditions. *Animal, 4*(8), 1390-1400. https://doi.org/10.1017/S1751731110000248

Aguerre, M. J., Wattiaux, M. A., Powell, J. M., Broderick, G. A., & Arndt, C. (2011). Effect of forage-to-concentrate ratio in dairy cow diets on emission of methane, carbon dioxide, and ammonia, lactation performance, and manure excretion. *J. Dairy Sci., 94*(6), 3081-3093. http://dx.doi.org/10.3168/jds.2010-4011

ANSYS. (2011). ANSYS Fluent. Ver. 14.0. Canonsburg, PA: ANSYS, Inc.

ASHRAE. (2009). *ASHRAE handbook of fundamentals*. Atlanta, GA: ASHRAE.

Calcmet. (2013). *Calcmet user's guide and reference manual*. Ver. 12.14. Helsinki, Finland: Gasmet Technologies Oy.

Charlesworth, P. S. (1988). *Air exchange rate and airtightness measurement techniques: An applications guide*. Coventry, U.K.: Air Infiltration and Ventilation Centre.

Freetly, H. C., & Brown-Brandl, T. M. (2013). Enteric methane production from beef cattle that vary in feed efficiency. *J. Animal Sci., 91*(10), 4826-4831. https://doi.org/10.2527/jas.2011-4781

Gilhespy, S., Webb, J., Retter, A., & Chadwick, D. (2006). Dependence of ammonia emissions from housing on the time cattle spent inside. *J. Environ. Qual., 35*(5), 1659-1667. https://doi.org/10.2134/jeq2005.0294

Grainger, C., Clarke, T., McGinn, S. M., Auldist, M. J., Beauchemin, K. A., Hannah, M. C., ... Eckard, R. J. (2007). Methane emissions from dairy cows measured using the sulfur hexafluoride tracer and chamber techniques. *J. Dairy Sci., 90*(6), 2755-2766. https://doi.org/10.3168/jds.2006-697

Kim, J., Maiti, A., Lin, L. C., Stolaroff, J. K., Smit, B., & Aines, R. D. (2013). New materials for methane capture from dilute and medium-concentration sources. *Nature Comm., 4*, article 1694. http://dx.doi.org/10.1038/ncomms2697

Knapp, J. R., Laur, G. L., Vadas, P. A., Weiss, W. P., & Tricarico, J. M. (2014). Invited review: Enteric methane in dairy cattle production: Quantifying the opportunities and impact of reducing emissions. *J. Dairy Sci., 97*(6), 3231-3261. https://doi.org/10.3168/jds.2013-7234

Lefcourt, A. M. (2001). Large environmental chamber: Ammonia recovery calibration. *Appl. Eng. Agric., 17*(5), 683-689. https://doi.org/10.13031/2013.6914

Lefcourt, A. M., Buell, B., & Tasch, U. (2001). Large environmental chamber: Design and operating characteristics. *Appl. Eng. Agric., 17*(5), 691-701. https://doi.org/10.13031/2013.6915

Maia, C. D. N., Ramirez, B. C., Green, A. R., Rodriquez, L. F., Segres, J. R., Shike, D. W., & Gates, R. S. (2015). A novel ruminant emission measurement system: Part I. Design evaluation and description. *Trans. ASABE, 58*(3), 749-762. https://doi.org/10.13031/trans.58.10752

MATLAB. (2015). Ver. 2015a. Natick, MA: The Mathworks, Inc.

Melse, R. W., & Timmerman, M. (2009). Sustainable intensive livestock production demands manure and exhaust air treatment technologies. *Bioresour. Tech., 100*(22), 5506-5511. http://dx.doi.org/10.1016/j.biortech.2009.03.003

Ndegwa, P. M., Hristov, A. N., Arogo, J., & Sheffield, R. E. (2008). A review of ammonia emission mitigation techniques for concentrated animal feeding operations. *Biosyst. Eng., 100*(4), 453-469. http://dx.doi.org/10.1016/j.biosystemseng.2008.05.010

Nienaber, J. A., & Maddy, A. L. (1985). Temperature-controlled multiple-chamber indirect calorimeter: Design and operation. *Trans. ASAE, 28*(2), 555-560. https://doi.org/10.13031/2013.32297

Norton, T., Sun, D.-W., Grant, J., Fallon, R., & Dodd, V. (2007). Applications of computational fluid dynamics (CFD) in the modelling and design of ventilation systems in the agricultural industry: A review. *Bioresour. Tech., 98*(12), 2386-2414. http://dx.doi.org/10.1016/j.biortech.2006.11.025

Place, S. E., Pan, Y., Zhao, Y., & Mitloehner, F. M. (2011). Construction and operation of a ventilated hood system for measuring greenhouse gas and volatile organic compound emissions from cattle. *Animals, 1*(4), 433. https://doi.org/10.3390/ani1040433

Pope III, C. A., Ezzati, M., & Dockery, D. W. (2009). Fine-particulate air pollution and life expectancy in the United States. *New England J. Med., 360*(4), 376-386. https://doi.org/10.1056/NEJMsa0805646

Powell, J. M., Broderick, G. A., & Misselbrook, T. H. (2008a). Seasonal diet affects ammonia emissions from tie-stall dairy barns. *J. Dairy Sci., 91*(2), 857-869. https://doi.org/10.3168/jds.2007-0588

Powell, J. M., Cusick, P. R., Misselbrook, T. H., & Holmes, B. J. (2007). Design and calibration of chambers for measuring ammonia emissions from tie-stall dairy barns. *Trans. ASABE, 50*(3), 1045-1051. https://doi.org/10.13031/2013.23145

Powell, J. M., Misselbrook, T. H., & Casler, M. D. (2008b). Season and bedding impacts on ammonia emissions from tie-stall dairy barns. *J. Environ. Qual., 37*(1), 7-15. https://doi.org/10.2134/jeq2007.0282

Purswell, J. L., Gates, R. S., Lawrence, L. M., Jacob, J. D., Stombaugh, T. S., & Coleman, R. J. (2006). Air exchange rate in a horse trailer during road transport. *Trans. ASABE, 49*(1), 193-201. https://doi.org/10.13031/2013.20238

Taylor, B. N., & Kuyatt, C. E. (1994). Guidelines for evaluating and expressing the uncertainty of NIST measurement results. NIST Tech. Note 1297. Gaithersburg, MA: National Institute for Standards and Technology.

TÜV Rheinland. (2013). Certificate of product conformity (QUAL1). Certificate No. 0000001031_01. Cologne, Germany: TÜV Rheinland Energie and Unwelt GmbH.

Yoon, S., Carey, J. N., & Semrau, J. D. (2009). Feasibility of atmospheric methane removal using methanotrophic biotrickling filters. *Appl. Microbiol. Biotech., 83*(5), 949-956. https://doi.org/10.1007/s00253-009-1977-9